

EVIDENCE FOR MERGER REMNANTS IN EARLY-TYPE HOST GALAXIES OF LOW-REDSHIFT QSO¹

Nicola Bennert², Gabriela Canalizo^{2,3}, Bruno Jungwiert^{2,4}, Alan Stockton⁵, François Schweizer⁶, Chien Y. Peng^{7,8}, Mark Lacy⁹

ABSTRACT

We present results from a pilot *HST* ACS deep imaging study in broad-band V of five low-redshift QSO host galaxies classified in the literature as ellipticals. The aim of our study is to determine whether these early-type hosts formed at high redshift and have since evolved passively, or whether they have undergone relatively recent mergers that may be related to the triggering of the nuclear activity. We perform two-dimensional modeling of the light distributions to analyze the host galaxies' morphology. We find that, while each host galaxy is reasonably well fitted by a de Vaucouleurs profile, the majority of them (4/5) reveal significant fine structure such as shells and tidal tails. These structures contribute between $\sim 5\%$ and 10% to the total V -band luminosity of each host galaxy within a region of $r \sim 3 r_{\text{eff}}$ and are indicative of merger events that occurred between a few hundred Myr and a Gyr ago. These timescales are comparable to starburst ages in the QSO hosts previously inferred from Keck spectroscopy. Our results thus support a consistent scenario in which most of the QSO host galaxies suffered mergers with accompanying starbursts that likely also triggered the QSO activity in some way, but we are also left with considerable uncertainty on physical mechanisms that might have delayed this triggering for several hundred Myr after the merger.

Subject headings: galaxies: active – galaxies: interactions — galaxies: evolution — quasars: general

¹Based on observations made with the NASA/ESA *Hubble Space Telescope*, obtained at the Space Telescope Science Institute, which is operated by the Association of Universities for Research in Astronomy, Inc., under NASA contract NAS 5-26555. These observations are associated with program # GO-10421.

²Institute of Geophysics and Planetary Physics, University of California, Riverside, CA 92521; nicola.bennert@ucr.edu, gabriela.canalizo@ucr.edu, bruno.jungwiert@ucr.edu

³Department of Physics and Astronomy, University of California, Riverside, CA 92521

⁴Astronomical Institute, Academy of Sciences of the Czech Republic, Boční II 1401, 141 31 Prague 4, Czech Republic

⁵Institute for Astronomy, University of Hawaii, 2680 Woodlawn Drive, Honolulu, HI 96822; stockton@ifa.hawaii.edu

⁶Carnegie Observatories, 813 Santa Barbara Street, Pasadena, CA 91101; schweizer@ociw.edu

⁷Space Telescope Science Institute, 3700 San Martin Drive, Baltimore, MD 21218

⁸NRC Herzberg Institute of Astrophysics, 5071 West

1. INTRODUCTION

Quasi-stellar objects (QSOs) are the most luminous active galactic nuclei (AGNs), believed to be powered by accreting supermassive black holes (BH). The growing observational evidence that massive BHs exist not only in the centers of active galaxies, but also in inactive early-type galaxies indicates that more than the mere presence of a massive BH is needed to trigger the activity. And while the “bright quasar phase” is now often cited as an essential phase in the evolution of galaxies (e.g., Springel et al. 2005a), we still do not have a clear picture of what causes the triggering, or even what the necessary conditions are for the triggering to occur.

Saanich Road, Victoria, British Columbia, Canada V9E 2E7; cyp@nrc-cnrc.gc.ca

⁹*Spitzer* Science Center, California Institute of Technology, Pasadena, CA 91125; mlacy@ipac.caltech.edu

For more than two decades now, mergers have been suspected to be responsible for triggering QSOs (Stockton 1982; Sanders et al. 1988). There is an abundance of circumstantial evidence in the literature connecting QSO activity at low redshifts with mergers and interactions (e.g., Heckman et al. 1984; Hutchings et al. 1988; Canalizo & Stockton 2001; Urrutia et al. 2007). Not only do a number of low-redshift QSOs show signs of interactions and mergers, but there is also a tendency for QSO host galaxies to exist in only moderately rich environments (e.g., Dressler et al. 1985; Ellingson et al. 1991; Wold et al. 2001, see, however, Martini et al. 2007 for a counterexample) consistent with the results of quasar clustering studies, which suggests that quasars exist in haloes of mass $\sim 10^{12} - 10^{13} M_{\odot}$ (Hopkins et al. 2007; da Angela et al. 2007). In such environments, velocity dispersions are moderate, and interactions have their greatest effect.

At least in the case of QSOs found in ultra-luminous infrared galaxies (ULIRGs), there is a close connection between mergers and QSO activity. ULIRGs are essentially always found in merging systems (Sanders & Mirabel 1996), and far too many of them harbor QSOs to be explained by the joint probability of finding a given L^* or brighter galaxy to be both a ULIRG and a QSO host galaxy by chance (Canalizo & Stockton 2001). So, at least for this subclass of QSO, some of the gas that the merger feeds into the central starburst also finds its way much deeper to the central black hole.

Nevertheless, recent high-resolution imaging studies show that a large fraction of QSOs reside in hosts with relaxed morphologies like elliptical galaxies (e.g., Disney et al. 1995; Bahcall et al. 1997; McLure et al. 1999; Floyd et al. 2004). These observations have elicited claims that tidal interactions in QSO host galaxies are the exception rather than the rule, and that even in those cases in which there are clear signs of interaction, the interactions are not necessarily related to the nuclear activity (e.g., Dunlop et al. 2003, hereafter D03). From two-dimensional fitting of a well matched sample of 33 AGNs (radio-loud and radio-quiet QSOs as well as radio galaxies), using images obtained with the Wide Field & Planetary Camera 2 (WFPC2) on board *HST*, D03 concluded that “for nuclear luminosities $M_V < -23.5$,

the hosts of both radio-loud *and* radio-quiet AGN are virtually all massive elliptical galaxies with basic properties that are indistinguishable from those of quiescent, evolved, low-redshift ellipticals of comparable mass”.

Such conclusions conflict with recent findings of significant amounts of dust and cold molecular gas, as well as young stellar populations, in many radio-loud and radio-quiet QSOs (e.g. Martel et al. 1999; Canalizo & Stockton 2001; Evans et al. 2001; Scoville et al. 2003; Tadhunter et al. 2005; Barthel 2006). Although the hosts of most luminous AGNs are bulge-dominated, they seem to be significantly bluer than inactive elliptical galaxies and indeed show evidence for starbursts in the relatively recent past (1–2 Gyr) (e.g., Kauffmann et al. 2003; Sánchez et al. 2004; Canalizo et al. 2006; Schweitzer et al. 2006; Jahnke et al. 2007).

In addition, both numerical simulations and observations show that merger remnants that have undergone violent relaxation have surface-brightness profiles that follow $r^{1/4}$ laws (e.g., Toomre & Toomre 1972; Barnes 1988; Hibbard & van Gorkum 1996), even while still showing clear signs of the tidal interactions (Rothberg & Joseph 2004). Thus, if QSO host galaxies are indeed relatively recent merger remnants, they would most likely have elliptical profiles, but they would also show fine structure indicative of past interactions.

Detecting fine structure in the already elusive QSO host galaxies is a challenging task. Studies of nearby merger remnants show that their fine structure is often faint compared to the galaxies themselves. For example, the total luminosity of the shells in shell galaxies accounts only for 5–15% of the total luminosity of the galaxy (e.g., Fort et al. 1986; Prieur 1988; Wilkinson et al. 2000), and their detection often requires a resolution of at least ~ 0.5 kpc (e.g., Schweizer & Seitzer 1992). Therefore, detecting fine structure in QSO hosts requires high angular resolution and higher signal-to-noise (S/N) observations than those obtained in previous studies.

Thus, we are conducting a study with deep (5 orbit) HST ACS and WFPC2 observations of a sample of QSO host galaxies that are classified as ellipticals. We presented results for the first object in Canalizo et al. (2007, hereafter Paper I). In the present paper, we describe results for the

four remaining objects from our pilot ACS study of 5 objects. We will present results for the rest of the sample (14 additional objects) in subsequent papers. Throughout this paper, we adopt $\Omega_\lambda = 0.7$, $\Omega_m = 0.3$ and $H_0 = 71 \text{ km s}^{-1} \text{ Mpc}^{-1}$.

2. SAMPLE SELECTION

Since the goal of our project is to investigate the possibility that QSO host galaxies are formed through mergers even when they do not show dramatic signs of tidal interactions, we should ideally draw our sample from a sample of hosts that have been classified as undisturbed elliptical galaxies. The best such sample is that of D03.

From the detailed morphological study of radio-loud and radio-quiet QSO host galaxies by D03, we selected QSOs for which the host galaxies were classified as elliptical galaxies¹. Moreover, we selected those objects for which existing deep Keck spectra did not reveal extended emission lines that could contaminate our observations in the broad V -band filter (F606W). We chose a sample of five QSOs, three radio-quiet and two radio-loud. The sample properties are summarized in Table 1.

3. OBSERVATIONS AND DATA REDUCTION

All observations were obtained using the ACS Wide Field Channel (WFC) onboard the *HST* with the broad V -band F606W filter ($\Delta\lambda = 2342\text{\AA}$; 1 pixel corresponds to $0.05''$). Five sets of dithered images were taken (with four subsets of 485–588 s integration time each), yielding a total integration time of 10740–11464 s per target (see Table 1).

In order to achieve background-limited images enabling us to detect any existing faint structure in the QSO host galaxies, we obtained individual frames with long integration times. Consequently, the central pixels of the QSO nuclei are saturated in these images. We discuss the effects of the saturation in detail in the next section.

We re-calibrated the data manually, correcting the pipeline flat-fielded single exposures for

¹Note that the D03 radio-loud and radio-quiet QSOs were selected to be statistically indistinguishable in their optical luminosity and redshift.

the bias-level offset between the adjacent quadrants that is still present in the final product of CALACS (Pavlovsky et al. 2005). We used MultiDrizzle (Koekemoer et al. 2002) to combine the individual images to the final distortion and cosmic-ray corrected scientific image (default values plus bits=8578 and a deltashift file with the offsets between the images as determined from stars within the field-of-view (FOV)). Note that no sky subtraction was performed during MultiDrizzle.

4. IMAGE ANALYSIS

Different methods such as unsharp masking, creating a structure map (Pogge & Martini 2002), and using the two-dimensional galaxy fitting program GALFIT (Peng et al. 2002) were applied to look for any fine structure that might be present. We here describe only the procedure we adopted for the use of GALFIT as the other two methods did not yield additional information (see Paper I for details on these methods).

For convolution with the point-spread function (PSF) of the *HST* ACS optics, we created both an artificial PSF star from TinyTim² (Version 6.3) at the same position as each QSO and a PSF star from an observed star on an ACS/WFC F606W image observed close to the positions of the QSOs. For the TinyTim PSF, we adopted a power law $F_\nu = \nu^\alpha$ with $\alpha = -0.3$ which is the average value we obtain for the QSOs.³ The computed radius for this artificial PSF is $10''$.

For the observed PSF star, we chose a star with a signal-to-noise ratio (S/N) of 20,000 from the *HST* archive. The star was observed on 20 dithered images with a total exposure time of $\sim 8100\text{s}$ (GO-9433, data sets j6mf19* and j6mf21*) and at a position of the WFC chip less than $5''$ away from the position of each QSO; note that the full ACS FOV is $3.4' \times 3.4'$. These images were processed in the same manner as described above for the QSO observations. Finally, we eliminated a few faint objects surrounding the PSF star and modified the PSF image to minimize any noise introduced during PSF subtraction and con-

²Available at <http://www.stsci.edu/software/tinytim/tinytim.html>

³ $(B - R)$ ranges between 0.1 and 0.7 as measured from nuclear Keck spectra.

TABLE 1
DETAILS OF OBSERVATION

QSO	IAU designation	α (J2000) (hh mm ss)	δ (J2000) ($^{\circ}$ ' '')	z	Type	Exp. Time (sec)	scale (kpc/'')
(1)	(2)	(3)	(4)	(5)	(6)	(7)	(8)
PHL 909	0054+144	00 57 09.9	+14 46 10	0.172	RQQ	10920	2.885
PKS 0736+01	0736+017	07 39 18.0	+01 37 05	0.191	RLQ	11364	3.137
PG 0923+201	0923+201	09 25 54.7	+19 54 05	0.190	RQQ	11464	3.124
MC2 1635+119	1635+119	16 37 46.5	+11 49 49	0.146	RQQ	11432	2.520
OX 169	2141+175	21 43 35.5	+17 43 49	0.211	RLQ	10740	3.392

NOTE.—Col. (1): QSO. Col. (2): IAU designation. Col. (3,4): Optical positions taken from NED. Col. (5): Heliocentric redshift as listed in NED. Col. (6): Classification as either radio-quiet QSO (RQQ) or radio-loud QSO (RLQ). Col. (7): Total integration time in sec. Col. (8): Physical scale in kpc/''.

olution procedures. To adaptively smooth the PSF, we compared data values to the standard deviation s of the surrounding sky: (1) for data values $> 7s$, we retained the unmodified PSF; (2) for data values between $3s$ and $7s$, the image was smoothed with a Gaussian kernel with $\sigma = 0.5$ pixel; (3) for data values $< 3s$, a Gaussian kernel of $\sigma = 2.0$ pixel was used, and (4) for data values $< 1s$ after this last operation, the value was replaced with 0. The radius of the observed PSF star is $\sim 4''$. The full-width-at-half-maximum (FWHM) of the PSF is $0.1''$ in both the artificial star and the observed PSF star, in close agreement with the FWHM of stars on the ACS images close to the QSO.

The observed PSF star has $(B - R) \simeq 1.4$ mag, as inferred from USNO⁴ data. To test chromatic effects on the form of the PSF, we created a series of artificial PSF stars using TinyTim. We used power laws with α ranging from -4.0 to 0.9, corresponding to $(B - R)$ values between 2 mag and 0 mag (to account for the observed range of $(B - R)$ of the QSOs and the star, plus possible uncertainties). We also created PSFs using a blackbody spectrum with temperatures between 3000 and 40000 K. We fitted these different PSFs and a host galaxy model to our QSOs. The derived host galaxy parameters vary by 2%. We thus consider the chromatic effects as negligible compared to the other uncertainties such as the PSF mismatch due to telescope or plate scale breathing, focus changes, PSF saturation (see below) etc.

We subtracted the two different PSFs (star and

TinyTim) from saturated and unsaturated stars within the ACS FOV, for comparison. The observed PSF star yielded significantly better results than the TinyTim PSF. Thus, we used the observed PSF star for all the subsequent fitting and, in the following, we simply refer to it as PSF or PSF star. This exercise also allowed us to estimate the quality of our PSF fit, taking into account the saturation of the QSO nucleus. The central region within a radius of $\sim 1.7''$ is strongly affected by the PSF subtraction. Any structure within this region may be an artifact.

We created artificial images to test the influence of the PSF saturation on the derived QSO host galaxy parameters. Since luminous quasars generally do not vary much over time scales of a few years, we can compare our quasar luminosities with D03 to estimate the degree of saturation in our images and the potential systematic errors that might arise due to saturation. This direct comparison shows that our AGNs may be saturated by as much as 60%. (Note that we define "60% saturation" in such a way that 60% of the flux is lost due to saturation.) In addition, we created model images where the AGN has the same luminosity as in D03. We then saturated the AGN by 60%. After masking out the central saturated pixels in the same manner as we analyzed our data (see below), we find that our systematic errors can be as large as 7% for the magnitude, 30% for the effective radius of the different host galaxy components and up to 30% for the Sérsic index. The PSF magnitude can be underestimated by up to 90% due to saturation. This explains the differences in AGN luminosity that we observe compared with

⁴United States Naval Observatory

D03 (see Table 2).

GALFIT (Peng et al. 2002) is a 2-dimensional fitting program based on χ^2 minimization; it allows the user to simultaneously fit one or more objects in an image with different model light distributions, such as Sérsi c (S rsi c 1968), de Vaucouleurs (de Vaucouleurs 1948), or exponential. The following steps were performed. We created a mask to exclude the saturated pixels in the center, the diffraction spikes, surrounding objects, and any visible fine structure in order to fit only the smooth underlying host galaxy light distribution. For the purpose of the χ^2 minimization, pixels were weighted by $1/\sigma^2$ with σ based on Poisson statistics as estimated by GALFIT. (Note that the weighting is however irrelevant for the central saturated pixel that were masked.) A PSF and a S rsi c function were fitted. We fitted the background sky and bright close neighboring galaxies simultaneously, while faint neighboring objects were simply masked. This least-square fit was then subtracted from the original image to obtain the residual image in which any fine structure superposed on the smooth host galaxy light distribution is more readily visible.

To estimate the uncertainties caused by the sky determination, we used two different approaches. First, different sizes of the fitting region were used (up to the largest possible size) with the sky varying freely. Second, the sky was also determined independently and held fixed to this value during alternative fits.

Note that a S rsi c power law is defined as

$$\Sigma(r) = \Sigma_{\text{eff}} \exp \left[-\kappa_n \left(\left(\frac{r}{r_{\text{eff}}} \right)^{1/n} - 1 \right) \right],$$

where Σ_{eff} is the pixel surface brightness at the effective radius r_{eff} , and n is the S rsi c index ($n = 4$ for a de Vaucouleurs profile, $n = 1$ for an exponential profile).

To fit the host galaxies, we used three different models: (1) a single de Vaucouleurs profile (S rsi c with $n = 4$), (2) a single S rsi c profile (n free) and (3) a combination of a de Vaucouleurs plus exponential (S rsi c with $n = 1$) profile. If the sky value is kept fixed during the fitting process, the fit for (1) has a total of nine free parameters: three parameters for the fitting of the PSF (α , δ , magnitude), and six free parameters

for the fitting of the de Vaucouleurs profile (α , δ , magnitude, r_{eff} , b/a , P.A.). Model (2) has one additional free parameter for the index n . Model (3) has six more free parameters than model (1). These parameters correspond to the exponential profile (α , δ , magnitude, r_{eff} , b/a , P.A.). In all three cases, if the sky is also fitted, there are three additional parameters (background and gradient in α and δ). In some cases, we used a S rsi c profile to fit bright galaxies in close proximity to the QSO hosts (PHL 909: six galaxies; PG 0923+201: seven galaxies, MC2 1635+119: one galaxy). In those cases, the free parameters for these fits add to the number of total free parameters.

5. HOST GALAXY PROPERTIES AND FINE STRUCTURE

In this section, we summarize the results for all five QSOs in the pilot sample. Although MC2 1635+119 was discussed in detail in Paper I, Figure 3 shows its luminosity profile which was not included in Paper I. To facilitate comparisons, we also include the results for MC2 1635+119 in the tables.

5.1. Host Galaxy Morphology

Figure 1 shows the ACS/WFC images for four of the five QSOs in our sample: PHL 909, PKS 0736+01, PG 0923+201, and OX 169. Including MC2 1635+119, four of the five host galaxies reveal extended fine structure on different scales and with different morphologies, ranging from spectacular shells and arcs (MC2 1635+119; Paper I), to tidal tails (PHL 909) to jet-like (OX 169) and spiral-like (PKS 0736+01) structure. Only one object (PG 0923+201) resides in a host galaxy without any obvious fine structure. We here describe the overall host-galaxy morphology for each object in turn. Further details on each object, including a comparison with results in the literature and a description of neighboring objects, are given in Appendix A.

The host galaxy of PHL 909 shows a variety of fine structures at different radii. A central ring- or disk-like structure ($r \simeq 1.8'' - 2.5''$) can be seen, possibly intersected by a dust lane to the SE (Fig. 1). To the NW, two shells are apparent. They occur at distances of $2.5''$ (P.A. $\simeq 328$) and $3''$ (P.A. $\simeq 298$). Diffuse outer material

seems to form another ring or disk-like structure (Fig. 4, inset; $r \simeq 3.4'' - 6''$). The most prominent fine structure consists of two tidal tails, one extending from the disk-like structure in the SE, curving towards the N, and the other extending from the disk in the NW, bending towards the south (Figs. 1 and 4). The western tidal tail extends to a galaxy (“a”; Fig. 4) $\simeq 16''$ to the NW (P.A. $\simeq 284^\circ$). The tidal feature most likely corresponds to the faint extended emission reported by McLure et al. (1999) which was also seen in the K-band image (Dunlop et al. 1993). The companion (“a”) itself has two tidal tails, one reaching out in the direction of the QSO and connecting with its tidal tail, another tidal tail extending to the S up to $5.5''$ (Fig. 1). Also the eastern tidal tail seems to be connected to a very faint small companion (“d”) at $14''$ distance from the QSO (P.A. $\simeq 98^\circ$), possibly a dwarf galaxy (Fig. 4, inset).

PKS0736+01 has been observed in the near-infrared K-band by Dunlop et al. (1993). The host is about $10''$ in diameter and is described as highly disturbed with a large area of low surface-brightness nebulosity and several compact companions embedded. In our deep *HST* ACS image, this nebulosity is clearly visible and shows resolved structure that looks like a faint face-on spiral. The spiral-like structure extends out to a radius of $16''$ ($\simeq 50$ kpc), i.e. very large for a normal spiral galaxy. Also, the pitch angle changes with radius, arguing against a simple spiral-arm interpretation. Instead, what is observed here, may be spatial wrapping of material from a merger event (see discussion in Sec. 6).

PG 0923+201 resides in a galaxy group of at least 6 galaxies, some of which form closely interacting pairs, including the two large elliptical galaxies to the south-east of the QSO (see Appendix A). However, the host galaxy itself does not reveal any obvious fine structure in the deep *HST* ACS image.

The host galaxy of MC2 1635+119 has been described in detail in Paper I. It reveals spectacular fine structure, consisting of (at least) five interleaved inner shells (out to $r \simeq 13$ kpc) and several extended arcs out to a radius of ~ 65 kpc.

The host galaxy of OX 169 exhibits an extended linear structure which has been reported by several authors (Stockton 1978; Hutchings et al. 1984; Gehren et al. 1984; Smith et al. 1986; Heckman et al.

1986). OX 169 was studied by Stockton & Farnham (1991) and Hutchings & Neff (1992) who described this jet-like structure in detail. Stockton & Farnham (1991) showed that it consists mainly of old stars at the same redshift. This is supported by the prominence of the structure also in the K-band image (Dunlop et al. 1993). While the feature resembles a galactic disk seen edge-on, with a dust lane in the SE, it is not centered on the QSO; almost 2/3 of it lies on the SE side of the QSO. Because of its strong asymmetry, Stockton & Farnham (1991) favor an interpretation as a tidal tail seen edge-on rather than a normal galactic disk. In our deep *HST* ACS image, the linear structure is very prominent and extends over a projected distance of ~ 68 kpc. The feature runs from NW to SE (P.A. $\simeq 303^\circ$), out to $\simeq 7.6''$ in the NW and $\simeq 12.5''$ in the SE. It is slightly curved and appears to continue across the nucleus. A dust lane is clearly visible between $7.6''$ and $11.5''$ in the SE side of the tail. In addition to the prominent linear structure, the deep *HST* ACS image reveals faint extended structure for the first time: a shell-like feature in the NE (P.A. $\simeq 83^\circ$) at a distance of $\simeq 5''$, plumes to the N of the SE end of the tail (P.A. $\simeq 110^\circ$) at a distance of $\simeq 11.5''$ from the center, and a fan extending from the SE tail towards the SW. The latter extends out to a companion (“a”; Fig. 4) to the SW (P.A. $\simeq 235^\circ$) at a distance of $6.1''$ and may be a tidal stream. The companion has an overall spiral-like morphology which seems to be tidally stretched. These findings provide strong support for the interpretation of the linear structure as a tidal tail seen edge on rather than it being a normal galactic disk. It is only natural to assume that all features have a common origin during a merger event.

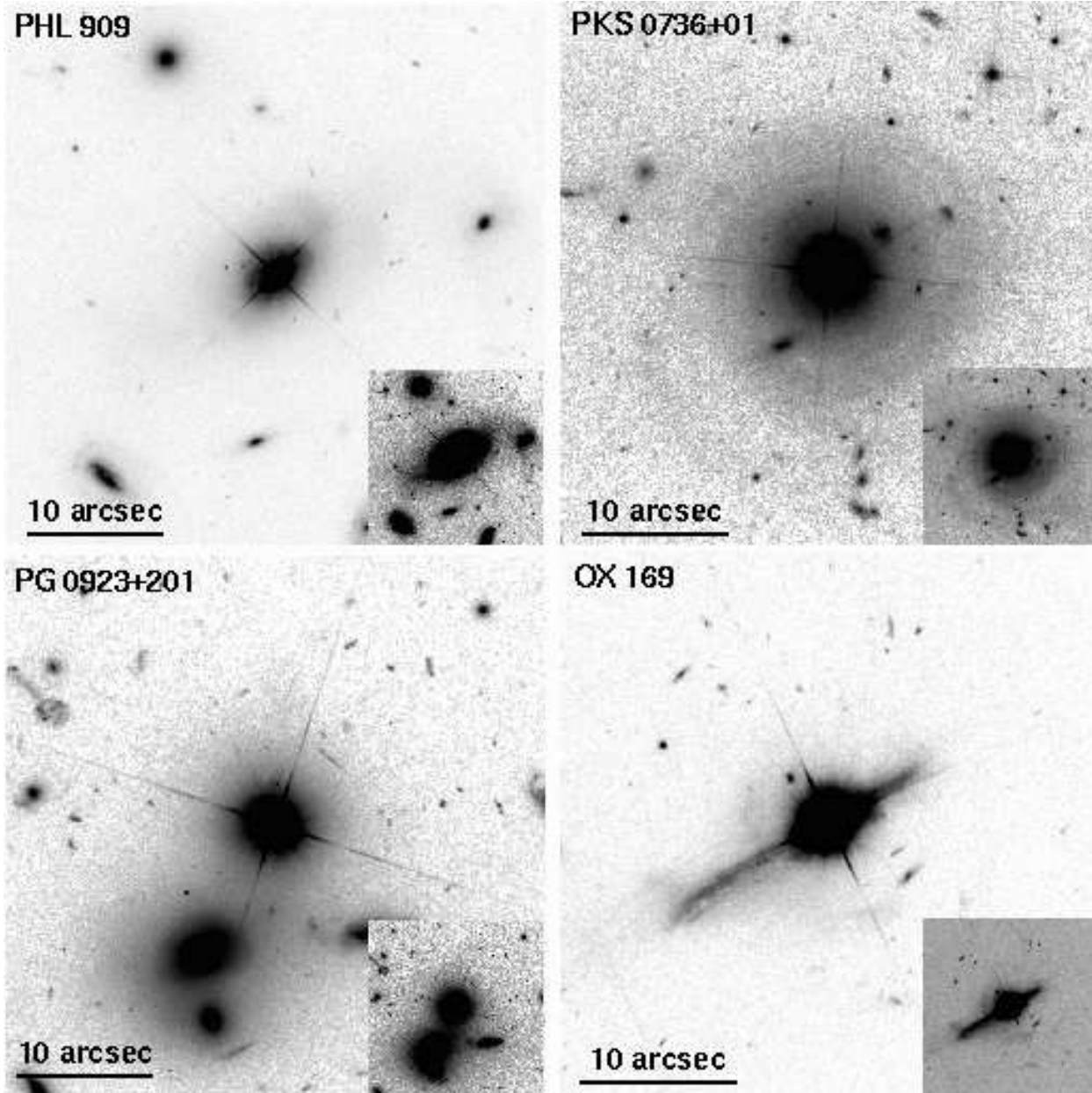


Fig. 1.— ACS/WFC images of four QSO host galaxies, all smoothed with a $\sigma = 0.5$ pixel Gaussian. In each image, north is up and east is to the left. A harder stretch is shown as inset, Gaussian smoothed with $\sigma = 1$ pixel (PHL 909, OX 169) and $\sigma = 2$ pixels (PKS 0736+01, PG 0923+201), respectively. Including MC2 1635+119 (Paper I), fine structure can be seen in at least four of the five QSO host galaxies (PHL 909: tidal tails and shells; PKS 0736+01: spiral-like structure; OX 169: disk-like structure, most likely tidal tail seen edge-on; MC2 1635+119: inner shells and outer arcs, see Paper I).

5.2. Host Galaxy Properties

As described in Section 4, we modeled the QSO host galaxies with GALFIT and fitted single de Vaucouleurs profiles, single Sérsic components, and a combination of de Vaucouleurs and exponential-disk profiles. Varying the range of the sky parameter shows that the uncertainty in photometry can be up to 20%, the uncertainty in r_{eff} up to 10%, and the uncertainty in Sérsic index up to 20%. These uncertainties add to the uncertainties from the PSF saturation (see Sec. 4). The total uncertainties are $\sim 20\%$ for photometry, $\sim 30\%$ in r_{eff} and $\sim 35\%$ in the Sérsic index. The results are summarized in Table 2.

For all objects, good fits were achieved with all three fitting functions mentioned above. The fits improved slightly in going from a single de Vaucouleurs to a single Sérsic to a combination of de Vaucouleurs plus exponential-disk profiles (see Table 2). While this is expected simply because of the increasing number of free parameters, the residual images do look smoother for the two-component fits. In such a decomposition, the de Vaucouleurs profile remains the dominant component, but the exponential-disk component contributes between 6% and 28% of the total luminosity in V of the hosts (Table 2). The residual image did improve significantly when adding a second component to the host in MC2 1635+119 (Paper I).

Single-Sérsic fits yielded a Sérsic index around 4 for each of the host galaxies (ranging between 2.9 and 6.5). Our results for the surface-brightness profiles of the underlying host galaxies are thus in overall agreement with those of Dunlop et al. (2003). In Figure 2, we show the residual images derived by subtracting a GALFIT model consisting of a single Sérsic profile from the observed images.

5.3. Surface-Brightness Profiles

We derived surface-brightness profiles for each object using the IRAF⁵ task *ellipse*. The profiles were obtained for both the observed surface brightness and the best-fitting model using GAL-

FIT and its subcomponents. The resulting 1D profiles for the different fits (single de Vaucouleurs, single Sérsic, de Vaucouleurs plus exponential) are only marginally different. Therefore, we only present the best fitting model using a Sérsic component in Figure 3.

The deviation of the model from the data within the central $1.7''$ is most likely caused by the PSF subtraction. This is especially pronounced for PG 0923+201, as this object has the brightest PSF (see Table 2), and the low S/N ratio in the outer parts of the PSF star results in additional noise in the data. In general, data points at a higher surface brightness than the model correspond to the fine structure that was masked out during GALFIT fitting but that was included for the creation of the 1D profiles. This is clearly the case for OX 169, for which the tidal tail causes the deviation between data and model beyond $5''$.

The surface-brightness plot of the observed host profile of PG 0923+201 shows a bump peaking around $2''$ that is not fitted by the model. Since this feature lies just outside of the central region that is affected by the PSF, we found it difficult to determine whether it is real or not. However, it could reflect the presence of an inner disk. If so, the outer radius of this disk would be approximately 8 kpc. The outer “uplift” of points over the best-fit profile (around $r \sim 8''$) is most likely due to the companion galaxy to the SSE and the relatively strong residuals that remain after subtracting the GALFIT model for this galaxy (see also Fig. 2). The observed surface brightness for PHL 909 also deviates slightly from the fit with a bump peaking around $2.3''$. This bump coincides with the ring-like structure seen in the image, with an outer radius of ~ 7 kpc.

⁵IRAF (Image Reduction and Analysis Facilities) is distributed by the National Optical Astronomy Observatories, which are operated by AURA, Inc., under cooperative agreement with the National Science Foundation.

TABLE 2
RESULTS OF MODELING THE QSO HOST GALAXIES USING GALFIT

QSO (fitted area) (1)	Model (2)	Function (3)	$\Delta(\alpha, \delta)$ (" , ") (4)	m_{F606W} (mag) (5)	R (mag) (6)	r_{eff} (") (7)	r_{eff} (kpc) (8)	Sérsi�c index (9)	b/a (10)	P.A. ($^\circ$) (11)	χ_ν^2 (12)
PHL 909 (950×950)	deV+Exp	PSF	(0,0)	17.23	4.83
		deV	(−0.1,−0.1)	17.08	...	2.35	6.77	4 (fixed)	0.57	130.4	...
		Exp	(−0.96,1.45)	19.88	...	3.14	9.05	1 (fixed)	0.57	111.0	...
	S	PSF	(0,0)	18.18	5.14
		S	(0.1,−0.06)	16.79	...	2.53	7.30	5.6	0.63	130.2	...
	deV	PSF	(0,0)	17.39	5.17
		deV	(−0.1,−0.05)	16.96	...	2.54	7.32	4 (fixed)	0.61	130.4	...
	deV (D03)	PSF	15.5
		deV	16.6	2.76	7.93	4 (fixed)	0.61	131
S (D03)	S	4	
PKS 0736+01 (1051×1051)	deV+Exp	PSF	(0,0)	17.18	2.20
		deV	(0.01,−0.05)	17.70	...	1.63	5.10	4 (fixed)	0.94	2.3	...
		Exp	(−0.94,−0.15)	18.75	...	7.09	22.23	1 (fixed)	0.80	86.2	...
	S	PSF	(0,0)	16.07	2.25
		S	(−0.04,0)	17.08	...	4.27	13.41	6.5	0.98	32.7	...
	deV	PSF	(0,0)	16.86	2.27
		deV	(−0.04,0)	17.35	...	3.30	10.34	4 (fixed)	0.98	39.2	...
	deV (D03)	PSF	16.2
		deV	16.9	3.27	10.21	4 (fixed)	0.97	26
S (D03)	S	5.3	
PG 0923+201 (1051×1051)	deV+Exp	PSF	(0,0)	16.39	2.59
		deV	(−0.04,−0.02)	17.40	...	1.44	4.49	4 (fixed)	0.96	174.2	...
		Exp	(1.02,0.75)	20.45	...	2.26	7.07	1 (fixed)	0.51	146.1	...
	S	PSF	(0,0)	16.15	2.76
		S	(0.07,−0.03)	17.48	...	1.81	5.66	2.9	0.97	42.1	...
	deV	PSF	(0,0)	16.36	2.78
		deV	(−0.06,0.01)	17.31	...	1.68	5.2	4 (fixed)	0.97	42.9	...
	deV (D03)	PSF	15.7
		deV	17.2	2.02	6.30	4 (fixed)	0.98	38
S (D03)	S	3.3	
MC2 1635+119 (481×481)	deV+Exp	PSF	(0,0)	17.58	3.49
		deV	(−0.03,0.04)	17.50	...	1.12	2.82	4 (fixed)	0.71	57.9	...
		Exp	(0.53,0.36)	18.81	...	5.48	13.8	1 (fixed)	0.82	27.7	...
	S	PSF	(0,0)	17.02	3.91
		S	(−0.03,0.04)	17.18	...	2.47	6.23	4.95	0.71	55.9	...
	deV	PSF	(0,0)	17.17	3.93
		deV	(−0.03,0.04)	17.27	...	2.05	5.16	4 (fixed)	0.71	56.2	...
	deV (D03)	PSF	18.1
		deV	16.8	2.28	5.73	4 (fixed)	0.69	56
S (D03)	S	5.6	

NOTE.—Col. (1): QSO and, in parentheses, the size of the fitted area in pixels. Col. (2) GALFIT model (deV = de Vaucouleurs, Exp = Exponential, S = Sérsi c). Col. (3): Individual components used. Col. (4): Offsets with respect to the PSF. Col. (5): Integrated apparent magnitude in the F606W filter. Note that the magnitudes m_{F606W} given for the PSF underestimate the AGN component as the PSF was saturated in all cases; see text for details. Col. (6): Integrated apparent magnitude converted from F675W to Cousins R band as given by D03. Col. (7,8): Effective radius in " and kpc, respectively. Note that although we concluded in Section 4 that the central region within a radius of $\sim 1.7''$ is still strongly affected by the PSF subtraction, all r_{eff} given in this table are more than 10 times the full-width-at-half-maximum (FWHM) of the ACS PSF. Col. (9): Sérsi c index. Col. (10): Axis ratio. Col. (11): Position angle (east of north). Col. (12): χ^2 per degree of freedom, ν . χ_ν^2 corresponds to the model in column 2. Results from D03 are listed for comparison. The r_{eff} given here for the D03 results were recalculated according to the worldmodel adopted in this paper. The P.A. given here for the D03 results were derived by adding the P.A. given in their Table 3 to the orientation of the spacecraft (as the P.A. given in their Table 3 is apparently not corrected for it).

TABLE 2 - CONTINUED

QSO (fitted area) (1)	Model (2)	Function (3)	$\Delta(\alpha, \delta)$ ("', ") (4)	m_{F606W} (mag) (5)	R (mag) (6)	r_{eff} ("' (7)	r_{eff} (kpc) (8)	Sérsić index (9)	b/a (10)	P.A. ($^{\circ}$) (11)	χ^2_{ν} (12)
OX 169 (900×900)	deV+Exp	PSF	(0,0)	17.80	3.45
		deV	(0,0)	17.68	...	1.82	6.17	4 (fixed)	0.47	120.4	...
		Exp	(0,0.15)	19.34	...	1.23	4.17	1 (fixed)	0.66	18.5	...
	S	PSF	(0,0)	17.54	3.66
		S	(0,0)	17.42	...	1.30	4.41	3.9	0.64	122.9	...
	deV	PSF	(0,0)	17.56	3.66
		deV	(0,0)	17.41	...	1.29	4.36	4 (fixed)	0.64	123.0	...
	deV (D03)	PSF	15.9
		deV	17.3	1.88	6.35	4 (fixed)	0.47	121	...
	S (D03)	S	3.6

NOTE.—Col. (1): QSO and, in parentheses, the size of the fitted area in pixels. Col. (2) GALFIT model (deV = de Vaucouleurs, Exp = Exponential, S = Sérsić). Col. (3): Individual components used. Col. (4): Offsets with respect to the PSF. Col. (5): Integrated apparent magnitude in the F606W filter. Note that the magnitudes m_{F606W} given for the PSF underestimate the AGN component as the PSF was saturated in all cases; see text for details. Col. (6): Integrated apparent magnitude converted from F675W to Cousins R band as given by D03. Col. (7,8): Effective radius in " and kpc, respectively. Note that although we concluded in Section 4 that the central region within a radius of $\sim 1.7''$ is still strongly affected by the PSF subtraction, all r_{eff} given in this table are more than 10 times the full-width-at-half-maximum (FWHM) of the ACS PSF. Col. (9): Sérsić index. Col. (10): Axis ratio. Col. (11): Position angle (east of north). Col. (12): χ^2_{ν} per degree of freedom, ν . χ^2_{ν} corresponds to the model in column 2.

Results from D03 are listed for comparison. The r_{eff} given here for the D03 results were recalculated according to the worldmodel adopted in this paper. The P.A. given here for the D03 results were derived by adding the P.A. given in their Table 3 to the orientation of the spacecraft (as the P.A. given in their Table 3 is apparently not corrected for it).

TABLE 3
CONTRIBUTION OF FINE STRUCTURE TO HOST GALAXY LIGHT

QSO (1)	fs ($3r_{\text{eff}}$) % (2)	Σ_{fs} ($3r_{\text{eff}}$) mag arcsec $^{-2}$ (3)	Σ_{fs} (max) mag arcsec $^{-2}$ (4)
PHL 909	7.8	29.2	24.8
PKS 0736+01	8.2	29.6	26.5
MC2 1635+119	6.3	28.3	25.2
OX 169	13.3	29.5	23.7

NOTE.—Col (1): QSO. Col. (2): Percentage of flux contained in the observed fine structure within $3r_{\text{eff}}$. Col. (3): Surface-brightness magnitude of the fine structure in the F606W filter within $3r_{\text{eff}}$. Col. (4): Average surface-brightness magnitude within an area of $2'' \times 2''$ around the maximum of the fine structure.

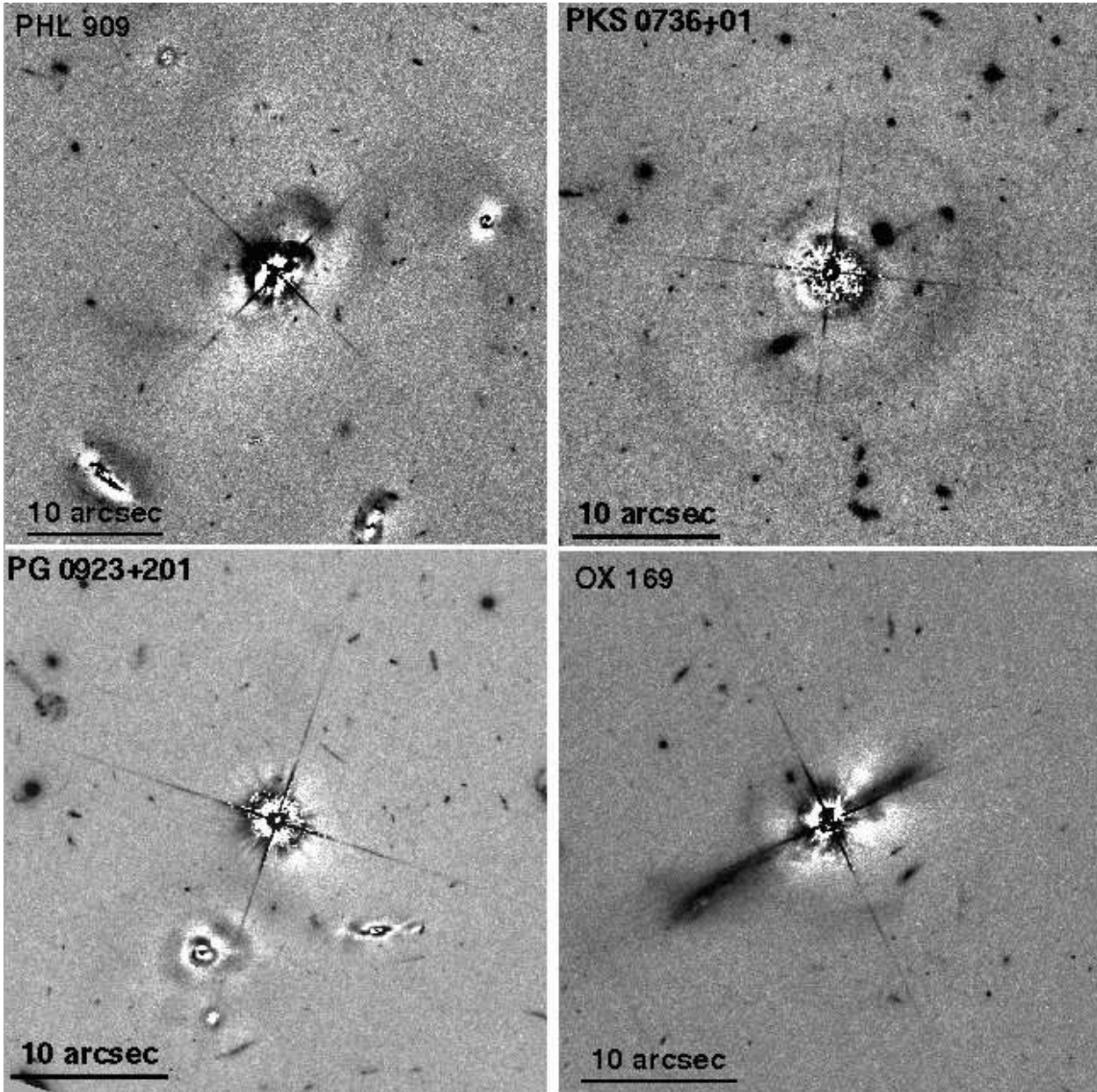


Fig. 2.— Residual images derived by subtracting a GALFIT model consisting of a single Sérsic profile. In each image, north is up, east is to the left. MC21635+119 was presented in Paper I.

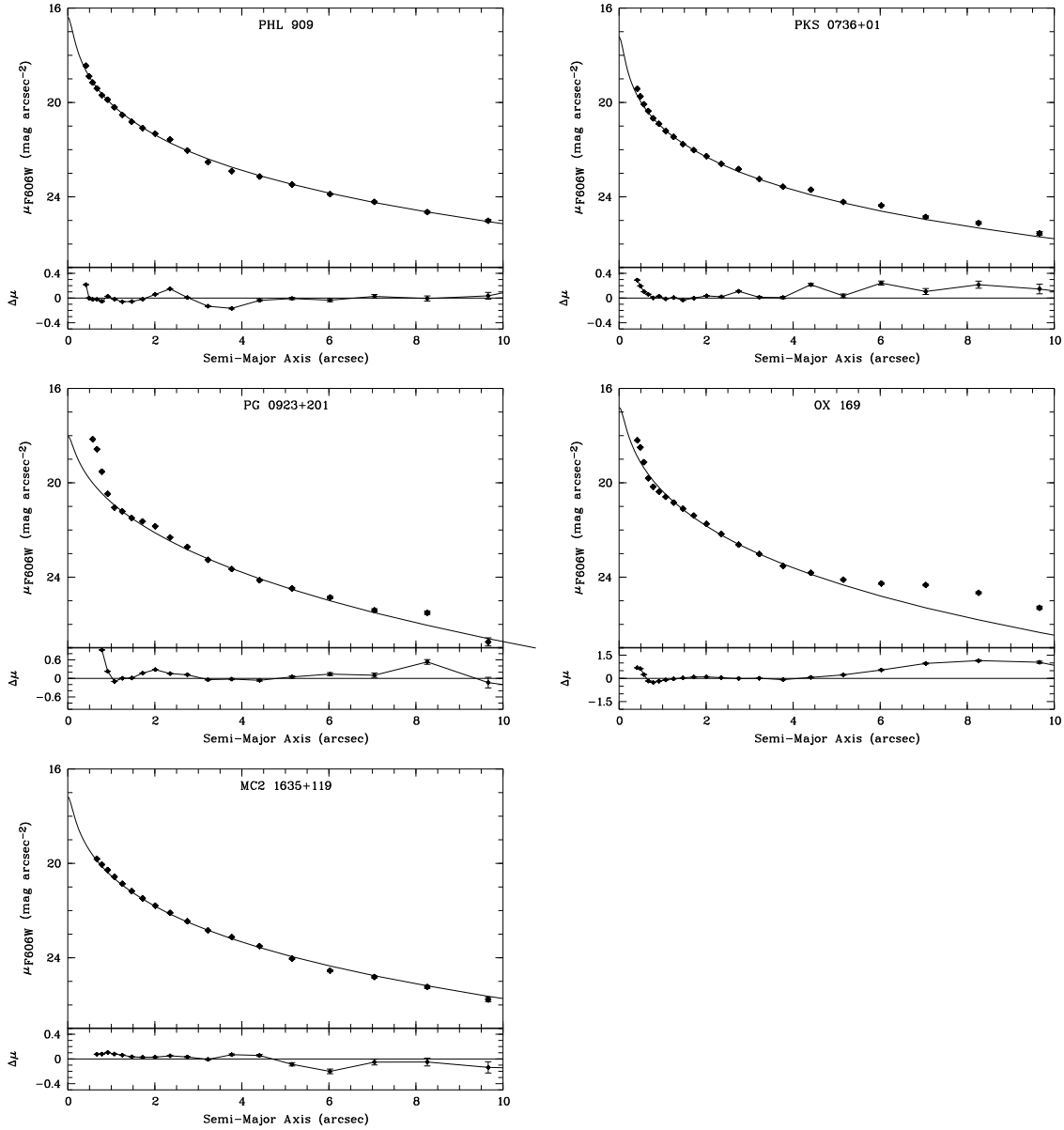


Fig. 3.— Surface-brightness plots of observed and best-fitting model profiles for all five QSO host galaxies. The observed profile is shown as diamonds with error bars. The resulting profile of fitting a single Sérsic profile is shown as a solid line. The residuals (fit – data) are shown in the lower panels.

5.4. Fine Structure

To estimate the luminosity within the various types of fine structure compared to the total luminosity of the host galaxy, we created a mask that included all the light within an annulus with an inner radius $1.7''$ and an outer radius $3r_{\text{eff}}$ (as taken from a single de Vaucouleurs fit, see Table 2). The image was multiplied by this mask (good=1, bad=0), and the total counts in the product were summed. This was done both for the GALFIT residual image ($f_{\text{finestructure}}$) obtained by subtracting the GALFIT model of a de Vaucouleurs + exponential profile, and for the GALFIT model itself (f_{galaxy}). We then computed the ratio $f_{\text{finestructure}}/f_{\text{galaxy}}$. The fractional luminosity of the extended fine structure in such an annulus ranges between 2% and 5%. To account for regions that were over-subtracted by GALFIT, we also used a slightly different approach: Applying the same general method as above, we only summed the pixels that are $> -1\sigma$ of the sky background. Then, the fractional luminosity of the extended fine structure ranges between 6% and 13%. The results are summarized in Table 3.

However, note that these values give only the average fraction within $3r_{\text{eff}}$. Locally, the surface-brightness magnitude of the fine structure relative to the underlying model can be much higher. The surface-brightness magnitude within an area of $2'' \times 2''$ centered on the maximum of the fine structure lies between ~ 24 and ~ 26 mag arcsec $^{-2}$ (as derived from the GALFIT residual image) for the four objects with fine structure (Table 3).

6. DISCUSSION

We find significant fine structure in the deep *HST* ACS images of at least four of the five QSO host galaxies (PHL 909, PKS 0736+01, MC2 1635+119, and OX 169) in our pilot sample. While the prominent linear structure in OX 169 has been previously reported by several authors (Stockton 1978; Hutchings et al. 1984; Gehren et al. 1984; Smith et al. 1986; Heckman et al. 1986; McLure et al. 1999), the structure in the other three objects is revealed here for the first time. Only one of the objects studied, PG 0923+201, does not show any obvious fine structure.

Our findings are supported by the WFPC2 im-

ages of D03 and McLure et al. (1999) since some of the structure that we find is also visible in their images: Part of the north-western tidal tail in PHL 909 is visible (Fig. A11, McLure et al. 1999); some of the spiral-like structure in PKS 0736+01 can be seen (Fig. A6 in McLure et al. 1999); and the shell in MC 1635+119 labeled “d” in Fig. 3 of Paper I is visible to the north-east of the QSO nucleus at a distance of $\sim 4''$ (Fig. A18 in McLure et al. 1999). However, the depth reached in our ACS images is needed to positively identify the “fuzz” seen in these earlier images as real. Our results clearly show the need of high S/N imaging for an accurate interpretation of QSO host galaxy morphologies.

The host galaxy of PG 0923+201 does not show obvious signs of fine structure. However, the surface-brightness profile reveals a bump in the inner $2''$ that could reflect the presence of an inner disk. Interestingly, PG 0923+201 resides in a galaxy group of at least 6 galaxies. It is the only QSO in our sample that has been observed with the *Spitzer* Space Telescope, both with the Infrared Spectrograph (IRS) and the Multiband Imaging Photometer for *Spitzer* (MIPS; $24\mu\text{m}$). Neither FIR emission nor Polycyclic-Aromatic Hydrocarbon (PAH) features have been detected (Shi et al. 2007). Interestingly, this lack of signs of star-formation activity in the infrared goes hand-in-hand with the lack of obvious signs for recent merger activity.

Much of the fine structure observed in our deep *HST* ACS images of the other four QSO host galaxies is indicative of merger events in the relatively recent past. The possible type and timescales for the merger in MC2 1635+119 were discussed in detail in Paper I. Briefly, we found that the fine structure seen in the host galaxy of this object was most likely produced by a strong tidal interaction within the last ~ 1 Gyr. On the one hand, the regularity of the inner shell structure is suggestive of a near radial collision of a dwarf galaxy with a giant elliptical galaxy in a minor merger. On the other hand, the arcs observed at much larger distances than the inner shells, and other tidal debris off-axis from the direction of the encounter implied by the inner shells, are more indicative of a major merger. Using simple N -body simulations, we estimated that the time scale needed to form the observed structure is less than

~ 1.7 Gyr (see Paper I for details). In comparison, the spectrum of the host galaxy is dominated by a population of intermediate-age (~ 1.4 Gyr) stars, indicative of a strong starburst that may have occurred during the merger event. Thus, the observed QSO activity may have been triggered in the recent past either by a minor merger or by debris from an older (\sim Gyr) major merger that is currently “raining” back into the central regions of the merger remnant.

The prominent extended structure observed in OX169 is most likely a tidal tail seen edge on. Prominent tidal tails are also observed in the host of PHL909. The tails in both QSO hosts are strongly suggestive of relatively recent major merger events, where at least some of the parent galaxies were disk galaxies.

The structure surrounding PKS0736+201 resembles that of the Seyfert 1.5 galaxy NGC5548, an Sa galaxy with ripples, tidal arms and a faint long tidal tail that has been described in detail by Schweizer & Seitzer (1988). The observed structure in NGC5548 has been interpreted in terms of the spatial wrapping of material from an obliquely infalling companion. When seen in projection, such material can appear in the form of relatively sharp-edged ripples (Schweizer & Seitzer 1988). Compared with NGC5548, the faint spiral-like structure seen in PKS0736+01 is more extended (~ 50 kpc vs. 10kpc) and more regular.

Structure similar to that observed in PKS0736+201 can be reproduced in numerical simulations of minor mergers. For example, the merger of a dwarf elliptical galaxy with a large spiral and a total mass ratio of 1:8 results in very similar structure ~ 1 Gyr after the first passage of the two galaxies, but also again at later stages in the merger event (Younger et al. 2007; T. J. Cox, private communication).

By comparing the structure observed in these hosts to results from numerous published N -body simulations of mergers (e.g., Hibbard & Mihos 1995), we know that the ages of these tidal features are likely of the order of a few orbital times. Given the masses of giant elliptical galaxies and the distances at which we observe these features, this time span ranges from a few hundred Myr to about 1 Gyr. In the cases in which we can clearly see tidal tails, we can infer that the dynamical timescales cannot be much less than ~ 250 Myr,

since that is roughly the amount of time that it would take for stars with typical orbital velocities (~ 200 km s $^{-1}$) to travel in a straight line to the projected maximum distances at which we observe the features (e.g., ~ 50 kpc for PHL909 or ~ 42 kpc for OX169). On timescales longer than ~ 1 Gyr, tidal tails are expected to rapidly disperse and lose contrast.

Further evidence that these are relatively evolved mergers is the fact that enough time has elapsed since the initial tidal encounter for each host to acquire an essentially elliptical morphology. While it is possible that some of the objects, such as MC1635+119 and PG0923+201, may have started off as elliptical galaxies, at least OX169 and PHL909 must have resulted from the merger of disk galaxies. The fact that they are at the present time reasonably well fitted by de Vaucouleurs profiles implies merger timescales on the order of a Gyr.

To address the question of whether the AGN activity may indeed have been triggered by the merger events, we need to obtain estimates of the different timescales involved. How do the ages of the stellar populations compare to the time elapsed since the merger events, and what does that imply for the QSO duty cycle? What is the connection between merger, star formation, and BH accretion?

As mentioned above, the timescales for the merger events observed in our sample is of the order of a Gyr or less. G. Canalizo & A. Stockton (2008, in preparation) find similar timescales for strong starburst events in the host galaxies of these QSOs. By modeling deep Keck spectra of these objects, they find traces of major starburst episodes in intermediate-age starburst populations that involve a substantial fraction of the stellar mass. These starburst ages range from ~ 0.7 Gyr (OX169) to 2.2 Gyr (PKS0736+017). Hence, it seems possible that the starbursts were triggered by the merger events.

The most difficult timescale to estimate is that of the duration of the AGN activity. Current estimates of QSO lifetimes range between 10^6 and 10^8 years and are derived primarily from demographics (see review by Martini 2004). For example, from theoretical calculations Yu & Tremaine (2002) estimate a mean lifetime for a luminous QSO ($L_{\text{bol}} \geq 10^{46}$ erg s $^{-1}$) of $(3-13) \times 10^7$ yr

which is comparable to the Salpeter time scale ($\sim 4.5 \times 10^7$ yr for $\epsilon = 0.1$ and $L/L_{\text{edd}} = 1$; Salpeter 1964; Martini 2004). Apart from demographics, there have been several attempts to deduce the AGN duty cycle for individual galaxies. For example, the length of radio jets can yield a lower estimate of QSO lifetimes, depending on the expansion speed of the jet (e.g., Willis & Strom 1978; Scheuer 1995; Blundell et al. 1999). However, this method cannot be applied to our sample as the two radio-loud QSOs in the sample each feature only a compact flat-spectrum radio source. Also, the size of the NLR has been proposed as a straightforward geometric measure of AGN lifetimes (Martini 2004). However, the NLR sizes for the five QSOs of our sample have not yet been determined.

Thus, as we do not have a direct way to estimate the time elapsed since the triggering of the nuclear activity for the objects in our sample, it is difficult to work out the physical relationship between the mergers we detect and the fueling of the QSOs. An overly simplistic scenario, in which each QSO was triggered by the merger at the time of the starburst episode would imply QSO lifetimes on the order of a Gyr, in stark contrast to the theoretical estimates cited above. Instead, our observations may provide evidence in support of significant time delays between tidal interactions and the fueling of the central black holes, as predicted by hydrodynamic simulations (see, e.g., Barnes 1998; Springel et al. 2005b; Hopkins et al. 2007).

However, while QSOs often reside in bulge-dominated galaxies like the ones presented in this study, they are also frequently found in young mergers (e.g., Urrutia et al. 2007; Guyon, Sanders & Stockton 2006; Canalizo & Stockton 2001; Hutchings et al. 1994). If, as the accumulating evidence suggests, mergers are indeed essential for the triggering of QSOs, then our results imply at least one of two scenarios: Either QSO activity is episodic (e.g., Norman & Scoville 1988; Hopkins et al. 2006) and occurs over longer timescales than previously speculated, or there is a large range of values for the time delays between the merger and the onset of the nuclear activity.

We thank the anonymous referee for the valuable comments helping to improve the paper. Support for the *HST* program 10421 was provided by NASA through a grant from the Space Telescope

Science Institute, which is operated by The Association of Universities for Research in Astronomy, Inc., under NASA contract No. NAS526555. Additional support was provided by the National Science Foundation, under grant AST 0507450. B. Jungwiert is also supported by the grant LC06014 of the Czech Ministry of Education and by Research Plan AV0Z10030501 of the Academy of Sciences of the Czech Republic. C. Y. Peng is grateful for support from the HIA Plaskett fellowship and the STScI Institute/Giacconi fellowship. This research has made use of the NASA/IPAC Extragalactic Database (NED) which is operated by the Jet Propulsion Laboratory, California Institute of Technology, under contract with the National Aeronautics and Space Administration.

A. NOTES ON INDIVIDUAL OBJECTS

Here, we give a more detailed description of each of the four QSOs. (Note that MC21635+119 was discussed in detail in Paper I.) Specifically, we review and discuss published data, compare them with our findings, and include a description of neighboring objects. The redshifts of companion galaxies and other galaxies within the ACS FOV are taken from NED unless stated otherwise. The full ACS/WFC images are shown in Figure 4, with labels for the galaxies to which we refer in the following discussion. Note that we cannot show detailed images for each such galaxy; instead, we refer the interested reader to the *HST* archive.

A.1. PHL 909

Based on older images, the host galaxy of the radio-quiet QSO PHL 909 ($z=0.172$, $1'' \simeq 2.89$ kpc) was described as an elliptical galaxy (Bahcall et al. 1996, 1997; Taylor et al. 1996; McLure et al. 1999; Hamilton et al. 2002). The age of the stellar population from off-nuclear optical spectra is not well constrained, but the spectra are suggestive of an old age (Nolan et al. 2001). Note, however, that Hughes et al. (2000) report a significant increase of flux bluewards of a weak 4000-Å break, but cannot determine whether it is due to scattered light from the QSO or indicative of a younger stellar population.

BH mass estimates (making use of σ , $\text{FWHM}_{\text{H}\beta}$ and L_{5100} , R -band luminosity of the host spheroid) cover a range of $0.17\text{--}2.5 \times 10^9 M_{\odot}$ (McLure & Dunlop 2001; Wu et al. 2002; Dunlop et al. 2003; Wu & Liu 2004). Dunlop et al. (2003) predict an Eddington ratio ($L_{\text{nuc}}/L_{\text{edd}}$) of 5.2%. Chun et al. (2006) classify PHL 909 as Lyman limit system. They mention a number of faint small objects surrounding the QSO that could be companions. In a K-band image, the galaxy extends $\sim 10''$ towards a western companion (Dunlop et al. 1993). The optical spectrum of PHL 909 shows double-peaked Balmer emission lines (Strateva et al. 2003). In the radio, PHL 909 is an unresolved point source (Kukula et al. 1998).

The arc-like features at $\simeq 2''$ from the QSO mentioned by Bahcall et al. (1996) correspond most likely to the central ring- or disk-like structure ($r \simeq 1.8'' - 2.5''$) seen in our deep *HST* ACS image. However, Bahcall et al. (1996) were unable to determine whether the features were artifacts due to the much lower S/N of their images.

The neighborhood of PHL 909 is populated with several objects, some of which look like dwarf galaxies. Seven brighter, nearby galaxies make PHL 909 appear to reside in a galaxy group. However, redshifts are known for only 3 objects, of which only one object is at the same redshift as the QSO, the large spiral galaxy (“h”) to the S (P.A. $\simeq 183^\circ$) $28''$ away ($z = 0.169$). The two other objects are foreground galaxies, one an elliptical galaxy (“b”; $z = 0.102$) to the NE (P.A. $\simeq 28^\circ$) at a distance of $18''$, and one a spiral (“e”; $z = 0.124$) to the SE (P.A. $\simeq 140^\circ$) $20''$ away. Two lenticular objects with unknown redshift lie at $31''$ E (“c”; P.A. $\simeq 96^\circ$) and $12''$ S (“f”; P.A. $\simeq 173^\circ$) projected distance of the QSO. A spiral galaxy to the SW (“g”; P.A. $\simeq 200^\circ$) is $20''$ away. Another bright object is the galaxy that is apparently interacting with the QSO (see Section 5.1). In the full FOV of the ACS frame (Fig. 4), redshifts are known for two other galaxies, both foreground spirals (“i”, $z = 0.104$, P.A. $\simeq 29.3^\circ$, distance $\simeq 1.12'$ and “j”, $z = 0.082$, P.A. $\simeq 76^\circ$, distance $\simeq 2.34'$).

A.2. PKS 0736+01

PKS 0736+01 ($z=0.191$, $1'' \simeq 3.14$ kpc) was classified as a blazar by Angel & Stockman (1980), as a compact flat-spectrum radio quasar by Wall & Peacock (1985), and as an optically violently variable by Brown et al. (1989). The host galaxy was described as an elliptical by Wright et al. (1998); McLure et al. (1999); Falomo & Ulrich (2000), and Hamilton et al. (2002). Off-nuclear optical spectra have been obtained and fitted by Hughes et al. (2000) and Nolan et al. (2001), indicating an age of 12 Gyr. The estimated BH mass (from relations with σ , $\text{FWHM}_{\text{H}\beta}$ and L_{5100} , R -band luminosity of the host spheroid) lies between 0.14 and $1.3 \times 10^9 M_{\odot}$ (McLure & Dunlop 2001; Wu et al. 2002; Dunlop et al. 2003). Dunlop et al. (2003) give 3.5% as an estimate of the Eddington ratio. The optical *HST* WFPC2 image of McLure et al. (1999) shows three companions (two to the NW and one to the SE), but fails to reveal the low surface-brightness

nebulosity, described as highly disturbed, seen in the K-band (Dunlop et al. 1993). In the near-infrared H-band, the host is resolved but round (Kotilainen et al. 1998).

Several faint objects surrounding PKS 0736+01 underlie the isophotes of the “spiral”. Two of these are background objects as determined from Keck spectra (G. Canalizo & A. Stockton 2008, in preparation): a lenticular-shaped galaxy at $5.9''$ to the SE (“a”; Fig. 4; P.A. $\simeq 147^\circ$; $z = 0.8500$) and an irregular galaxy at a distance of $4.4''$ to the NW (“b”; P.A. $\simeq 307^\circ$; $z = 0.3785$). The latter shows a tidal tail that is extending toward another object to the NW (“c”; P.A. $\simeq 297^\circ$; distance $\simeq 9''$) of unknown redshift.

Whether the observed faint spiral-like structure in PKS 0736+01 indeed indicates the presence of a faint spiral host galaxy, whether it is formed from debris of a merger event as speculated in Section 6, or whether it is actually a combination of both (a spiral disturbed by accreted material), our observations clearly show that the host galaxy of PKS 0736+01 cannot be considered to be an undisturbed elliptical galaxy.

A.3. PG 0923+201

The radio-quiet QSO PG 0923+201 ($z=0.19$, $1'' \simeq 3.12$ kpc) resides in an elliptical host galaxy (Bahcall et al. 1997; McLure et al. 1999, 2000; Hamilton et al. 2002; Guyon, Sanders & Stockton 2006). It is not detected as a radio source (Kukula et al. 1998). From a noisy optical off-nuclear spectrum, Nolan et al. (2001) estimate a stellar-population age of about 12 Gyr. BH mass estimates (using σ , $\text{FWHM}_{\text{H}\beta}$ and L_{5100} , R -band luminosity of the host spheroid) yield $M_{\text{BH}} \simeq 0.11\text{--}2.6 \times 10^9 M_\odot$ (McLure & Dunlop 2001; Wu et al. 2002; Dunlop et al. 2003). Dunlop et al. (2003) estimate an Eddington ratio $L_{\text{nuc}}/L_{\text{edd}}$ of 8.8%.

PG 0923+201 is a member of a galaxy group: In the ACS FOV, at least 5 galaxies are at a comparable redshift of $z \simeq 0.19$, (pair “a”, Heckman et al. (1984); “c”, Ellingson et al. (1991); pair “d”, Keck spectra; G. Canalizo & A. Stockton 2008, in preparation), four of which form two interacting pairs (“a”, “d”; Fig. 4). The closest pair (“a”) at $\sim 12''$ to the east consists of two large elliptical galaxies [one galaxy at $10''$ (P.A. $\simeq 153^\circ$) and one galaxy at $15''$ (P.A. $\simeq 161^\circ$) to the SE]. Hutchings et al. (1989) speculated that the QSO may be interacting with these. The northern galaxy of this pair shows a shell-like structure. The other pair (“d”) lies at a projected distance of $\simeq 1.6'$ to the north-east (P.A. $\simeq 21^\circ$). Both galaxies have clear tidal tails on one side and are connected by a tidal bridge. The fifth galaxy (“c”) at a comparable redshift lies $18''$ to the east (P.A. $\simeq 83^\circ$), a small galaxy with overall elliptical morphology but faint extended tail-like structures. The tidal tails make it resemble a more distant and faint version of the Antennae galaxies (NGC4038/4039), the best-studied and nearest (~ 19.2 Mpc) example of a major interaction between two massive gas-rich spiral galaxies. However, this object is possibly at a later stage of the merger as the two nuclei seem to have coalesced. The SE arm ends in a knot, a compact object that could be an interacting dwarf galaxy.

Note that within the ACS FOV, another galaxy pair (“e”) at a distance of $\simeq 2'$ to the east (P.A. $\simeq 92^\circ$) is at an advanced stage of merging, with curved tidal tails and the nuclei appearing disrupted in several fragments. While Ellingson et al. (1991) list this pair at a redshift of $z = 0.1899$, Keck spectra show that it is rather at a redshift of $z = 0.2318$ (G. Canalizo & A. Stockton 2008, in preparation). The redshift is known for one other galaxy within the ACS FOV, a background spiral (“f”, $z = 0.2328$, P.A. $\simeq 87^\circ$, distance $\simeq 2.6'$). There is another very close galaxy to the SW (P.A. $\simeq 224^\circ$) of the QSO, (“b”; distance $\simeq 11''$) with peculiar, tidally disrupted morphology, but unknown redshift.

There are at least two arcs close to the QSO (labeled as “1” and “2” in Fig. 4) that could be gravitationally lensed galaxies. However, they may also be tidal debris, especially in the case of “1”, which lies close to the interacting pair marked “a”.

A.4. OX 169

The host galaxy of the radio-loud QSO OX 169 ($z=0.211$, $1'' \simeq 3.39$ kpc) has been described as being an elliptical (Hutchings & Neff 1992; Taylor et al. 1996; McLure et al. 1999). Nolan et al. (2001) infer an old age for the stellar population of OX 169 from their optical off-nuclear spectrum, although the spectrum has a low S/N ratio. BH mass estimations using different relations (σ , $\text{FWHM}_{\text{H}\beta}$ and L_{5100} , R -band luminosity of the host spheroid) cover a range of $0.22\text{--}1.7 \times 10^9 M_\odot$ (McLure & Dunlop 2001; Wu et al. 2002; Dunlop et al.

2003). The Eddington ratio is estimated to be 6.1% (Dunlop et al. 2003). From its radio emission, OX 169 is classified as a compact ($< 4''$) flat-spectrum source (Feigelson et al. 1984).

OX 169 seems to have several faint satellite galaxies, but their redshifts are unknown. The closest one at $3.7''$ to the NE (“c”; P.A. $\simeq 43^\circ$) merges with the outer isophotes of the QSO host galaxy and resembles a dwarf elliptical galaxy. Two others lie towards the SW at distances of $4.6''$ (“b”; P.A. $\simeq 245^\circ$) and $6.1''$ (“a”; P.A. $\simeq 235^\circ$). The former has an irregular shape and resembles a tidally disrupted galaxy, while the latter object is the companion already described in Section 5.1.

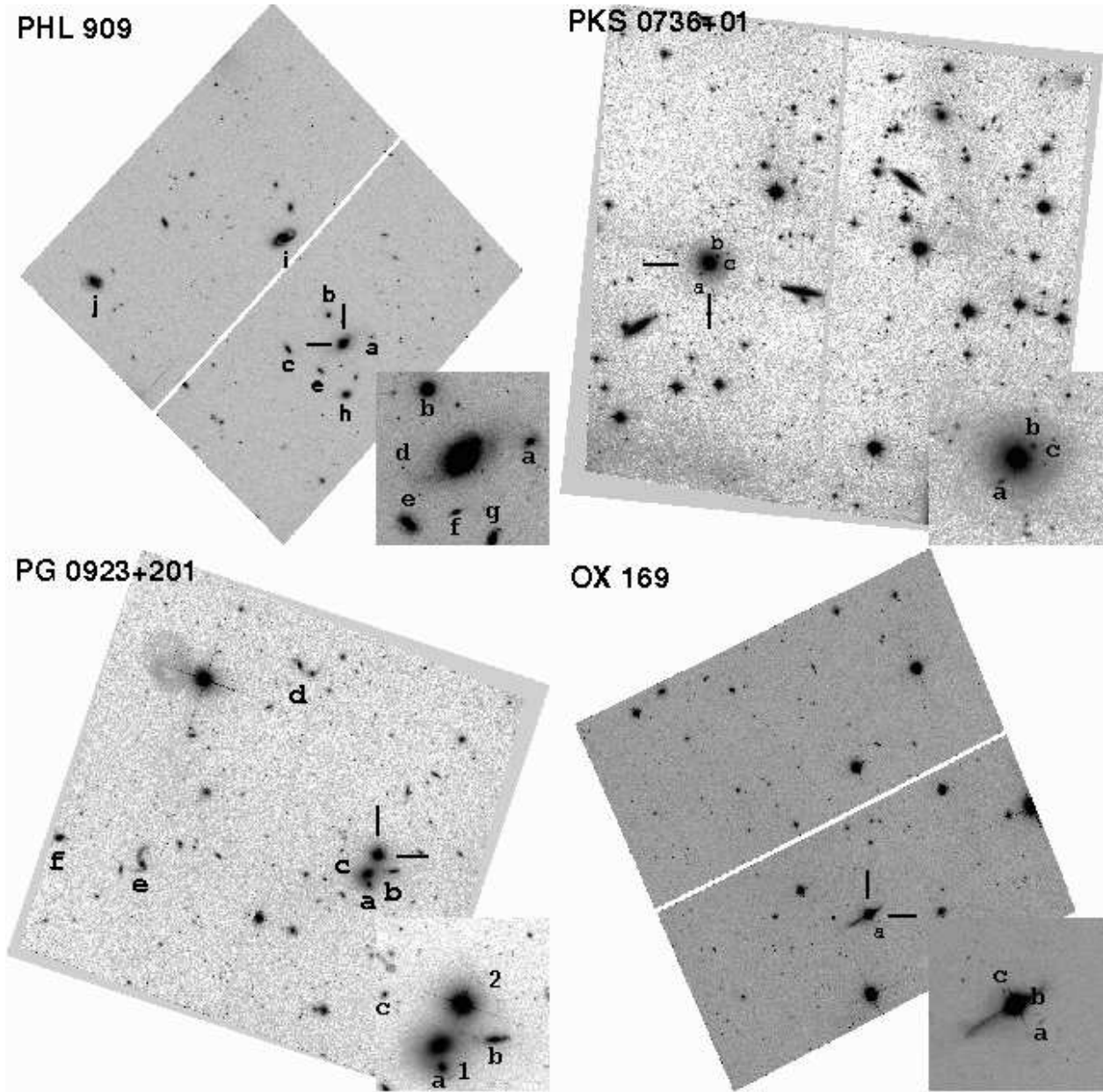


Fig. 4.— Full ACS/WFC images of four QSO host galaxies. The two bars mark the position of the QSO. North is up, east is to the left. The FOV of the ACS/WFC frame is $3.4' \times 3.4'$. As inset, a smaller area around each QSO is shown, with the image size identical to the images in Figs. 1 and 2. Letters mark the galaxies we refer to in the text. The letters refer to the closest object north or south of them. In the case of PG 0923+201, the two numbers refer to the arcs east of them.

REFERENCES

- Angel, J. R. P., & Stigma, H. S. 1980, *ARA&A*, 18, 321
- Bahcall, J. N., Kirhakos, S., & Schneider, D. P. 1996, *ApJ*, 457, 557
- Bahcall, J. N., Kirhakos, S., Saxe, D. H., & Schneider, D. P. 1997, *ApJ*, 479, 642
- Barnes, J. E. 1988, *ApJ*, 331, 699
- Barnes, J. E. 1998, in *Galaxies: Interactions and Induced Star Formation*, ed. Friedli, D., Martinet, L., & Pfenniger, D. (Berlin: Springer), 275
- Barthel, P. D. 2006, *A&A*, 458, 107
- Blundell, K. M., Rawlings, S., & Willot, C. J. 1999, *AJ*, 117, 677
- Brown, L. M. L., et al. 1989, *ApJ*, 340, 129
- Canalizo, G., & Stockton, A. 2001, *ApJ*, 555, 719
- Canalizo, G., Stockton, A., Brotherton, M. S., & Lacy, M. 2006, *NewAR*, 50, 650
- Canalizo, G., Bennert, N., Jungwiert, B., Stockton, A., Schweizer, F., Lacy, M., & Peng, C. 2007, *ApJ*, 669, 801
- Chun, M. R., Gharanfoli, S., Kulkarni, V. P., & Takamiya, M. 2006, *AJ*, 131, 686
- da Angela, J. et al. 2007, *MNRAS*, accepted (arXiv:astro-ph/0612401)
- de Vaucouleurs, G. 1948, *Ann. d'Astrophys.*, 11, 247
- Disney, M. J., et al. 1995, *Nature*, 376, 150
- Dressler, A., Thompson, I. B., & Sackett, S. A. 1985, *ApJ*, 288, 481
- Dunlop, J. S., Taylor, G. L., Hughes, D. H., & Robson, E. I. 1993, *MNRAS*, 264, 455
- Dunlop, J. S., McLure, R. J., Kukula, M. J., Baum, S. A., O'Dea, C. P., & Hughes, D. H. 2003, *MNRAS*, 340, 1095 (D03)
- Ellingson, E., Green, R. F., & Yee, H. K. C. 1991, *ApJ*, 378, 476
- Evans, A. S., Frayer, D. T., Surace, J. A., & Sanders, D. B. 2001, *AJ*, 121, 1893
- Falomo, R., & Ulrich, M.-H. 2000, *A&A*, 357, 91
- Feigelson, E. D., Isobe, T., & Kembhavi, A. 1984, *AJ*, 89, 1464
- Floyd, D. J. E., Kukula, M. J., Dunlop, J. S., McLure, R. J., Miller, L., Percival, W. J., Baum, S. A., & O'Dea, C. P. 2004, *MNRAS*, 355, 196
- Fort B. P., Prieur J.-L., Carter D., Meatheringham S. J. & Vigroux L., 1986, *ApJ*, 319, 110
- Gehren, T., Fried, J., Wehinger, P. A., & Wyckoff, S. 1984, *ApJ*, 278, 11
- Guyon, O., Sanders, D. B., & Stockton, A. 2006, *ApJS*, 166, 89
- Hamilton, T. S., Casertano, S., & Trunskel, D. A. 2002, *ApJ*, 576, 61
- Heckman, T. M., Bothun, G. D., Balick, B., & Smith, E. P. 1984, *ApJ*, 89, 7
- Heckman, T. M., Smith, E. P., Baum, S. A., van Breugel, W. J. M., Miley, G. K., Illingworth, G. D., Bothun, G. D., & Balick, B. 1986, *ApJ*, 311, 526
- Hibbard, J. E., & Mihos, J. C. 1995, *ApJ*, 110, 140
- Hibbard, J. E., & van Gorkom, J. H. 1996, *AJ*, 111, 655
- Hopkins, P. F., Hernquist, L., Cox, T. J., & Keres, D. 2007, *ApJ*, submitted (arXiv:0706.1243v2)
- Hopkins, P. F., Lidz, A., Hernquist, L., Coil, A. L., Myers, A. D., Cox, T. J., Spergel, D. N., *ApJ*, 662, 110
- Hopkins, P. F., Hernquist, L., Cox, T. J., Di Matteo, T., Robertson, B., & Springel, V. 2006, *ApJS*, 163, 1
- Hughes, D. H., Kukula, M. J., Dunlop, J. S., & Boroson, T. 2000, *MNRAS*, 316, 204
- Hutchings, J. B., Crampton, D., Campbell, B., Duncan, D., & Glendenning, B. 1984, *ApJS*, 55, 319

- Hutchings, J. B., Johnson, I., & Pyke, R. 1988, *ApJS*, 66, 361
- Hutchings, J. B., Janson, T., & Neff, S. G. 1989, *ApJ*, 342, 660
- Hutchings, J. B., & Neff, S. G. 1992, *AJ*, 104, 1
- Hutchings, J. B., Holtzman, J., Sparks, W. B., Morris, S. C., Hanisch, R. J., & Mo, J. 1994, *ApJ*, 429, L1
- Jahnke, K., Wisotzki, L., Courbin, F. & Letawe, G. 2007, *MNRAS*, 378, 23
- Kauffmann, G., et al. 2003, *MNRAS*, 346, 1055
- Koekemoer A. M., Fruchter, A. S., Hook, R. N., & Hack, W. 2002, in *Proc. 2002 HST Calibration Workshop*, ed. S. Arribas, A. Koekemoer, & B. Whitmore (Baltimore: STScI), 337
- Kotilainen, J. K., Falomo, R., & Scarpa, R. 1998, *A&A*, 332, 503
- Kukula, M. J., Dunlop, J. S., Hughes, D. H., & Rawlings, S. 1998, *MNRAS*, 297, 366
- Malkan, M. A. 1984, *ApJ*, 287, 555
- Martel, A. R., et al. 1999, *ApJS*, 122, 81
- Martini, P. 2004, *Coevolution of Black Holes and Galaxies*, from the Carnegie Observatories Centennial Symposia. Published by Cambridge University Press, as part of the Carnegie Observatories Astrophysics Series. Editor Ho, L. C. 2004, 169.
- Martini, P., Mulchaey, J. S., Kelson, D. D. 2007, *ApJ*, 664, 761
- McLure, R. J., Kukula, M. J., Dunlop, J. S., Baum, S. A., O’Dea, C. P., & Hughes, D. H. 1999, *MNRAS*, 308, 377
- McLure, R. J., Dunlop, J. S., & Kukula, M. J. 2000, *MNRAS*, 318, 693
- McLure, R. J., & Dunlop, J. S. 2001, *MNRAS*, 327, 199
- Nolan, L. A., Dunlop, J. S., Kukula, M. J., Hughes, D. H., Boroson, T. & Jimenez, R. 2001, *MNRAS*, 323, 308
- Norman, C. A., & Scoville, N. Z. 1988, *ApJ*, 332, 124
- Pavlovsky, C., et al. 2005, "ACS Data Handbook", Version 4.0, (Baltimore: STScI)
- Peng, C. Y., Ho, L. C., Impey, C. D., & Rix, H.-W. 2002, *AJ*, 124, 266
- Pogge, R. W., & Martini, P. 2002, *ApJ*, 569, 624
- Prieur J.-L., 1988, *ApJ*, 326, 596
- Rothberg, B. & Joseph, R.D. 2004, *ApJ*, 128, 2098
- Salpeter, E. E. 1964, *ApJ*, 140, 796
- Sánchez, S. F., et al. 2004, *ApJ*, 614, 586
- Sandage, A., & Bedke, J. 1994, *Carnegie Institution of Washington with The Flintridge Foundation*, Washington DC
- Sanders, D. B., Soifer, B. T., Elias, J. H., Madore, B. F., Matthews, K., Neugebauer, G., & Scoville, N. Z. 1988, *ApJ*, 325, 74
- Sanders, D. B., & Mirabel, I. F. 1996, *ARA&A*, 34, 749
- Scheuer, P. A. G. 1995, *MNRAS*, 277, 331
- Schweitzer, M., et al. 2006, *ApJ*, 649, 79
- Schweizer, F., 1980, *ApJ*, 237, 303
- Schweizer, F., & Seitzer, P. 1988, *ApJ*, 328, 88
- Schweizer, F., & Seitzer, P. 1992, *AJ*, 104, 1039
- Scoville, N. Z., Frayer, D. T., Schinnerer, E., & Christopher, M. 2003, *ApJ*, 585, L105
- SérsiĆ, J. L. 1968, *Atlas de Galaxias Australes* (Córdoba: Obs. Astron., Univ. Nac. Córdoba)
- Shi., Y., et al. 2007, *ApJ*, accepted (arXiv:0707.2806v1)
- Smith, E. P., Heckman, T. M., Bothun, G. D., Romanishin, W. & Balick, B. 1986, *ApJ*, 306, 64
- Springel, V., Di Matteo, T., Hernquist, L. 2005a, *ApJ*, 620, L79
- Springel, V., Di Matteo, T., Hernquist, L. 2005b, *MNRAS*, 361, 776

- Stockton, A. 1978, *ApJ*, 223, 747
- Stockton, A. 1982, *ApJ*, 257, 33
- Stockton, A., & Farnham, T. 1991, *ApJ*, 371, 525
- Strateva, I. V., Brandt, W. N., Eracleous, M., Schneider, D. P., & Chartas, G. 2003, *ApJ*, 651, 749
- Tadhunter, C., Robinson, T. G., González Delgado, R. M., Wills, K., & Morganti, R. 2005, *MNRAS*, 356, 480
- Taylor, G. L., Dunlop, J. S., Hughes, D. H., & Robson, E. I. 1996, *MNRAS*, 283, 930
- Toomre, A., & Toomre, J. 1972, *ApJ*, 178, 623
- Urrutia, T., Lacy M., & Becker, R. H. 2007, *ApJ*, in press (arXiv:0709.2805)
- Wake, D. A., et al. 2004, *ApJ*, 610, L85
- Wall, J. V., & Peacock, J. A. 1985, *MNRAS*, 216, 173
- Wilkinson, A., Prieur, J.-L., Lemoine, R., Carter, D., Malin, D., Sparks, W. B. 2000, *MNRAS*, 319, 977
- Willis, A. G., & Strom, R. G. 1978, *A&A*, 62, 375
- Wold, M., Lacy, M., Lilje, P. B., Serjeant, S. 2001, *MNRAS*, 323, 231
- Wright, S. C., McHardy, I. M., & Abraham, R. G. 1998, *MNRAS*, 295, 799
- Wu, X.-B., Liu, F. K., Zhang, T. Z. 2002, *A&A*, 389, 742
- Wu, X.-B., & Liu, F. K. 2004, *ApJ*, 614, 91
- Younger, J. D., Cox, T. J., Seth, A. C., & Hernquist, L. 2007, *ApJ*, accepted (arXiv:0707.4481v1)
- Yu, Q., & Tremaine, S. 2002, *MNRAS*, 335, 965